Tantalum Passive Persistence Shunts for On-Chip Current Trapping in Metallic Magnetic Calorimetry

Ruslan Hummatov, Linh N. Le, John A. Hall, Stephan Friedrich, Robin A. Cantor and S. T. P. Boyd

Abstract— Ultra-high resolution photon detectors based on Metallic Magnetic Calorimeters (MMCs) employ a weakly magnetized paramagnetic sensor to measure the energy of the absorbed particles. MMCs can require large on-chip magnetizing currents of order ~100 mA to achieve optimal performance. To minimize noise injected from room-temperature current supplies, it is useful to trap these currents in on-chip persistent superconducting loops. These loops have so far used electrically-heated persistent current switches. However, wire count can be reduced and design flexibility increased by using a passive superconducting persistent current switch with a T_c intermediate between T_c of the Nb loop and the operating temperature of the MMC. In addition, it is desirable for the T_c of the switch to be above the regeneration temperature on single-shot adiabatic demagnetization refrigerators (ADRs). We present passive persistent current switch measurements obtained with Ta film grown on a 100 Å Nb base layer. We have demonstrated trapping of up to 150 mA with no evidence of flux creep over 20 hours, and persistence of 100 mA trapped current through several regeneration cycles of our ADR with a regeneration temperature of ~2 K.

***Index Terms*—metallic magnetic calorimeter, persistent current switch, tantalum thin film**

I. Introduction

METALLIC Magnetic Calorimeters (MMCs) [1] are an important alternative to transition-edge-sensor (TES) microcalorimeters for high resolution photon and particle spectroscopy. MMCs already offer energy resolution comparable to TESs, and their underlying physics gives MMCs important advantages: 1) Magnetization is an equilibrium thermodynamic property, so microfabrication process variation has less impact on detector performance. 2) Detector behavior can be accurately predicted from first principles before fabrication. 3) No bias power is required by MMC sensors, which reduces noise and allows scaling to large arrays. 4) Electron-phonon and electron-spin thermalization times can be extremely fast, yielding pulse rise times faster than 0.1 μs at 100 mK.

A schematic of an MMC is shown in Fig. 1. It consists of a particle absorber with a paramagnetic sensor in a small magnetizing field and a SQUID magnetometer. When a particle is absorbed, the temperature of the absorber and paramagnetic sensor increases in proportion to the particle energy, and the magnetization of the sensor decreases. This magnetization change is transferred to the SQUID by using a superconducting flux transformer as shown, or can be measured directly within the SQUID loop. The energy of the particle is estimated with high precision from the amplitude of the resulting SQUID signal.

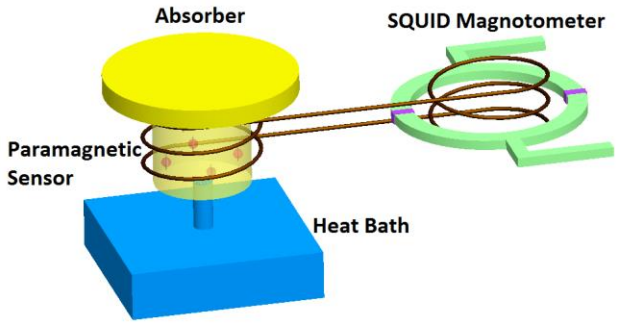

Fig. 1. Main components of an MMC particle detector.

For optimum performance with our current MMC designs for gamma-ray spectroscopy, the static magnetizing field applied to the paramagnet needs to be approximately 10 mT. With our typical spiral magnetizing coil designs this level of magnetizing field requires on-chip currents of order 100 mA. Although these magnetizing currents can successfully be supplied from a current source at room temperature, for optimal current stability and noise isolation the magnetizing current should be a trapped persistent current in an on-chip superconducting loop.

Thin film persistent current switches using on-chip resistance heaters to drive a short length of the superconducting traces above the superconducting critical temperature T_c have been used since 1994 [2,3]. A typical persistent-current circuit consists of a magnetizing coil with inductance L_{Coil} in parallel with a persistence shunt with inductance $L_{Shunt} \ll L_{Coil}$ (Fig. 2a). When the circuit is fully superconducting, any current applied to the terminals is distributed in inverse proportion to L_{Coil} and L_{Shunt}, so the majority simply passes through the shunt. To trap current in the magnetizing coil, a current is applied to the heater

Automatically generated dates of receipt and acceptance will be placed here; authors do not produce these dates. Work supported in part by the U.S. Department of Energy under Grant LL16 MagMicro PD1La. This work was performed under the auspices of the U.S. Department of Energy by Lawrence Livermore National Laboratory under Contract DE-AC52-07NA27344.

Ruslan Hummatov, Linh N. Le and Stephen T. P. Boyd are with the Department of Physics and Astronomy, University of New Mexico, Albuquerque, NM 87131 (e-mail: hummatov@unm.edu; linhle@unm.edu; stpboyd@unm.edu).

John A. Hall and Robin A. Cantor are with STAR Cryoelectronics, Santa Fe, NM 87508 (e-mail: ahall@starcryo.com; rcantor@starcryo.com).

Stephan Friedrich is with the Lawrence Livermore National Laboratory, Livermore, CA 94550 USA (e-mail: friedrich1@llnl.gov).

terminals to heat the shunt above its T_c and force the current through the magnetizing coil. When the heater current is turned off, the circuit becomes fully superconducting again, but now with zero current in the shunt. Finally, the applied current I is withdrawn, and conservation of flux in the superconducting loop establishes a persistent loop current of magnitude $I{\cdot}L_{Coil}/(L_{Coil}+L_{Shunt})$.

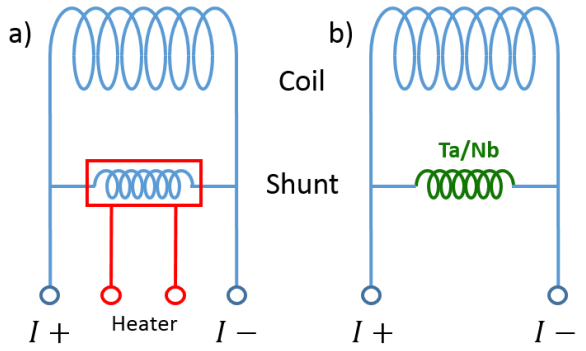

Fig. 2. (a) Schematic of heater-controlled persistent current switch. The rectangle represents the resistance heater. (b) Diagram of critical temperature controlled passive persistence shunt.

This approach to persistent current trapping in MMCs has been demonstrated by both the Heidelberg and UNM MMC groups [4-8]. However, the resistance-heater switch increases wire count. Further, if it is desired to have multiple persistent current switches for a multi-pixel MMC detector, or to eliminate inadvertent current trapping into SQUID input circuits, the requirement for additional on-chip heater wiring can considerably complicate the design and introduce potential noise sources.

An alternative approach to persistent current switches that eliminates heaters and their associated wiring was introduced by the NASA/GSFC MMC group [9]. More recently this new approach has been pursued by the Korean MMC group [10], motivated by the large number of separate MMC detectors required for the AMoRE experiment [11], and the large wire count that resistive heater persistent current switches would create. As shown in Fig. 2(b), the resistive heater can be eliminated by using a different superconducting material for the persistence shunt with T_c lower than the T_c of the wiring and the coil (typically Nb, T_c = 9.3 K) but higher than the MMC operating temperature (typically < 100 mK). A modified version of the current trapping procedure is now used: 1) the temperature of the device is held between the T_c of the shunt and the T_c of the wiring and the coil. 2) Current is applied to the terminals. 3) The device is cooled below T_c of the shunt. 4) The applied current is withdrawn. With this approach any number of persistence shunts can be incorporated into an MMC pixel array with almost no impact on layout complexity, and no concern about additional noise from heater wiring.

For a microfabrication process using niobium wiring layers, the T_c persistence shunt can readily be implemented by using an aluminum wire bond to complete an on-chip superconducting loop. This has been demonstrated by the NASA/GSFC group with 25 mA [9] and by the Korean MMC group for currents up to 80 mA [10]. The aluminum wire-bond, with T_c near 1.2 K, is a feasible approach for dilution-refrigerator-mounted experiments that will be maintained continuously at the MMC operating temperature. However, it is desirable to have a micro-fabricated shunt to reduce the parasitic inductance and possible noise pickup of the wire bonds due to increased loop area compared to a fully microfabricated MMC. Further, in cryostats cooled by a single-shot ADR it is desirable to have the shunt T_c above the regeneration temperature of the ADR in order not to lose the trapped current every time the ADR is regenerated.

For these reasons the Korean MMC group tested current trapping with a micro-fabricated shunt made of MoGe alloy and recently achieved trapping of 7 mA [10]. The low critical current was attributed to poor step-edge coverage of the MoGe over their Nb wiring.

In this report we describe our investigation of passive persistence shunts using tantalum. Bulk Ta has T_c = 4.47 K, close to typical ADR regeneration temperatures, is long-term stable, and is known from previous work to be entirely compatible with the STAR Cryoelectronics [12] SQUID microfabrication process, which is the foundation of our MMC process.

Superconducting properties of thin-film Ta have been investigated in the context of superconducting tunnel-junction (STJ) photon detectors [13-17]. Good superconducting performance of sputtered Ta films depends critically on the presence of an Nb underlayer. Without that Nb underlayer, sputter-deposited Ta does not form the bulk crystal phase and has very low T_c.

The T_c of deposited Ta films with Nb underlayer is a strong function of the thickness of the underlayer, and can exceed the T_c of bulk Ta for thick underlayers. Thus these films are more properly described as bilayers rather than as homogeneous Ta, with the expectation that T_c and current distributions may vary through the thickness of the bilayer.

II. EXPERIMENT

To investigate the performance of Ta/Nb bilayers as persistence shunts, a two-mask wafer of test devices was fabricated. Starting with a Si wafer coated with 400 nm of thermal SiO_2, the first mask defined a 500 nm sputtered Nb wiring layer patterned with RIE. The persistence shunt bilayer was then created by sputtering 10 nm Nb followed by 157 nm Ta through the second mask without breaking vacuum. The persistence shunt structures were patterned with liftoff. The 10 nm Nb underlayer thickness was chosen to target T_c near 5 K, based on the published STJ research and unpublished measurements previously performed at STAR Cryoelectronics as part of developing their commercial STJ x-ray spectrometer [16-18].

Test devices from the fabricated wafer were of two types: 1) meanders of both Ta/Nb and Nb, and 2) Nb loops shunted by Ta/Nb bilayers. The meander devices were used to measure the temperature dependence of the superconducting critical current $I_c(T)$. Persistence-shunted loop devices were used to test current trapping and flux creep.

The persistence-shunted loop device and its measurement setup are seen in Fig. 3. The on-chip Nb loop was circular, with trace width 10 μm and a 1 mm loop diameter. The persistence shunt spanned the 10 μm gap between the two Nb bonding pads and had width 100 μm.

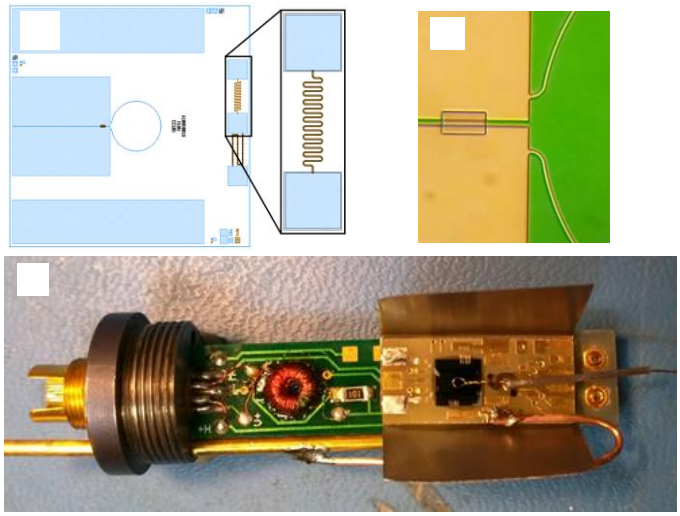

Fig. 3. Persistence-shunted loop device and its measurement setup. **(a)** device layout. The inset shows detail of a meander device for $I_c(T)$ testing **(b)** optical micrograph of persistence shunt joining the bond pads. **(c)** Persistence-shunted loop device attached to Conductus SQUID. The 1 mm dia wire pickup coil is centered above the on-chip magnetizing coil.

The chip was attached to a carrier PC board. Three Al wire bonds provided electrical connection between each current-injection bonding pad on the chip to the corresponding gold plated copper trace on the carrier. Those traces on the carrier were subsequently tinned with superconducting eutectic PbSn solder to reduce resistive length. The chip was heat-sunk via 5 Al wire bonds from heat-sinking pads to corresponding pads on the carrier. Heat sinking from the carrier to the ADR was via a thick copper wire. Al wire bonds provided adequate heat sinking for the chip, as the minimum measurement temperature of ~1 K is only slightly below T_c for Al.

A compact measurement setup was then realized by attaching the PC board carrier directly to the circuit board of an older Conductus SQUID [19] as shown in Fig. 3(c). The SQUID was shielded from the magnetic fields of the test device and its wiring by wrapping the device in NbTi foil before attachment. The wire pickup loop was attached to the SQUID input screw terminals via a length of twisted pair enclosed in a superconducting tube. This compact measurement setup could then be entirely contained within the Nb shield of the Conductus SQUID.

In the course of performing the measurements we discovered that this particular model of Conductus SQUID was manufactured with Mo shunt resistors, setting a lower limit of about 0.8 K to its operating temperature range.

III. Results and Discussion

A. Current-Carrying Capacities

Each measurement of $I_c(T)$ was performed by first stabilizing a meander device at constant temperature with zero applied current, then increasing the applied current until a voltage drop appeared in the 4-wire measurement. Note that in these measurements we were not trying to determine the maximum current-carrying capacity of the trace under ideal conditions. Rather, we are trying to determine engineering limits in a practical configuration similar to an MMC device.

Fig. 4 shows measured $I_c(T)$ for Nb and Ta/Nb meanders. This data confirms that T_c for the bilayers is indeed close to the targeted 5 K. We are interested in two current-capacity limits from this plot: the current capacity of Nb traces at the current injection temperature just above the T_c of the Ta/Nb bilayer, and the current capacity of the Ta/Nb bilayer at the ADR regeneration temperature. We see that a 10 μm-wide Nb trace can carry about 200 mA near the shunt T_c. For an ADR regeneration temperature of 2 K (the UNM ADR, which regenerates against a 1 K pot) a 30 (60) μm-wide shunt is required to support a magnetizing current of 100 (200) mA. For a more-typical ADR regeneration temperature of 4 K, a ~135 μm-wide shunt is required to support a magnetizing current of 100 mA. These limits create little or no constraint on our optimized sensing coil designs, which typically use magnetizing traces of width 10 μm or larger and can easily accommodate these shunt lengths.

The steep rise in $I_c(T)$ for the 10 μm-wide Nb trace at the lowest temperatures appears to be due to the disappearance of Joule heating in the aluminum wire bonds below their superconducting transition. This idea is supported by the appearance of a small voltage increase near the T_c of Al before the meander itself went normal, corresponding to about 5 mΩ resistance through the tripled Al wire bonds. The absence of the steep rise in $I_c(T)$ at lower currents presumably reflects the more-favorable balance between the heat-sinking of the chip and the I^2 dependence of Joule heating in the wire bonds. Note that the electrical resistance of the Al wire bonds has no impact on the on-chip trapped persistent current—it only impacts injection and withdrawal of that current.

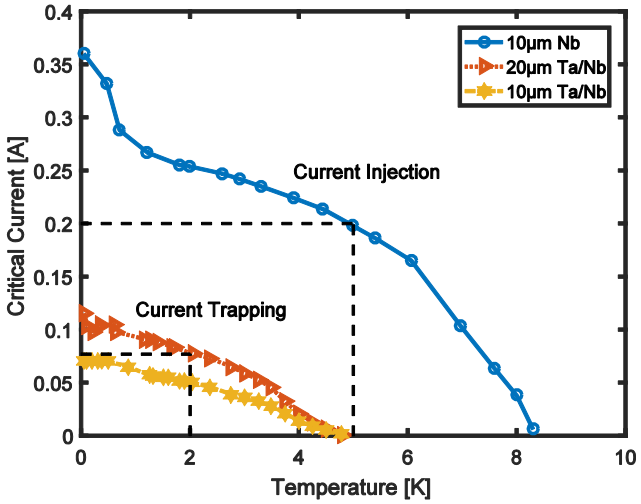

Fig. 4. Measured superconducting critical current $I_c(T)$ of Nb and Ta/Nb meanders with widths as indicated.

B. *Trapping of Persistent Currents*

Current-trapping was measured via SQUID magnetometry. The large diameter of the on-chip Nb loop was chosen to allow good flux coupling to an off-chip 1 mm-diameter pickup loop hand-wound from 100 μm diameter superconducting wire. This allowed the current in the on-chip loop to be easily monitored by a simple SQUID magnetometer setup. As shown in Fig. 3(b) the Nb/Ta shunt used in these tests was 100 μm wide.

Typical current trapping data is shown in Fig. 5. The sequence of operations for trapping and releasing the current is described in the figure's caption. As shown in the inset, the SQUID signal change during current injection (1-2) and current decay (5-6) are equal and proportional to the amount of current up to 150 mA, demonstrating successful current trapping. At 200 mA, the constant of proportionality was reduced, and the SQUID signal change for decay (5-6) fell well below the change for injection (1-2). We speculate that this behavior is due to un-tracked flux jumps occurring at higher field stress.

The form of the curves is as expected, with two exceptions. The features in the SQUID signal seen in segment (2-3) were seen even when the test chip was removed from the SQUID, so we assign them to superconducting transitions associated with the materials of the Conductus SQUID, rather than anything germane to this measurement. Other than these features, the SQUID signal due to temperature changes with the test chip removed was found to be negligible.

It may seem surprising that the linear ramp in segment (3-4), when the external current was withdrawn, has the same "polarity" as the linear ramp (1-2) when the external current was applied. This indicates that the principal impact of the current withdrawal at 1 K on the SQUID signal is via the redistribution of the current from the leads to the shunt, as the current in the shunt is expected to strengthen the SQUID signal. For our measurement setup, this effect outweighs the previously-described decrease in trapped current that must occur upon withdrawal of the applied current. However, investigating the detailed balance between these effects is beyond the scope of the present measurement.

C. *Flux Creep*

To ensure that an MMC fitted with these passive persistence shunts will have stable calibration, flux creep through the persistence shunt was tested via a modification to the data-taking procedure shown in Fig. 5. Namely, after withdrawal of the externally-applied current at point (4), the test device was maintained at a controlled temperature for an extended period of time, with the SQUID signal providing a continuous monitoring of the trapped current. A number of these tests were performed. In the most stringent case, 150 mA was trapped at 1 K for 20 hours. This test showed no measureable change in the flux coupled to the SQUID.

Further testing was performed to check for sensitivity of the trapped current to ADR operation. 100 mA was trapped for 9 hours during which 3 ADR regeneration cycles were performed. In this case the ~50 mK temperatures reached by the ADR fell below the 0.8 K minimum operating temperature of the Conductus SQUID (this model has Mo shunt resistors), so continuous SQUID monitoring was not possible. However, when the temperature was finally raised at the end of the test the current decay signal (5-6 in Fig. 5) agreed with the expected current release, confirming that the trapped current can withstand the mechanical and electrical disturbances associated with closing and opening our solenoid-driven heat switch.

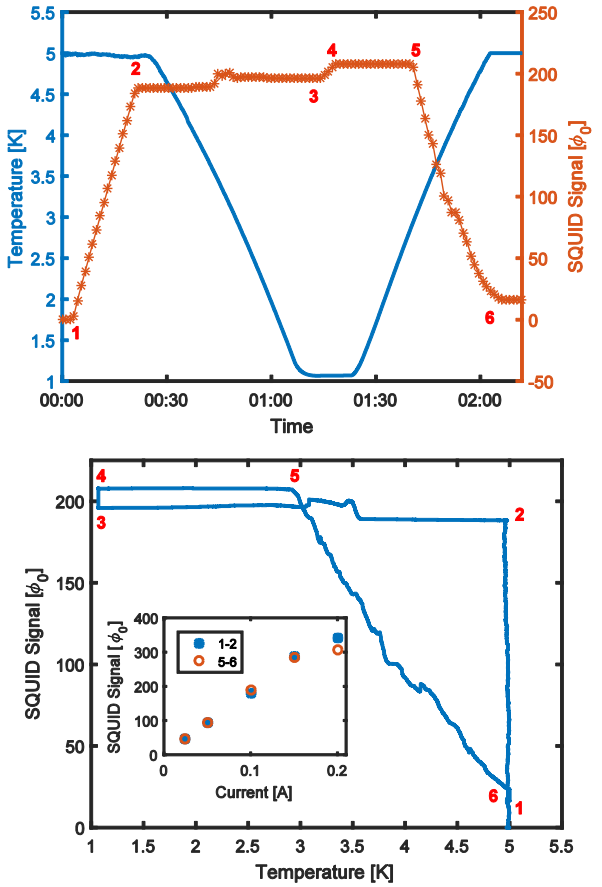

Fig. 5. Measured temperature (no markers) and SQUID output signal (markers) for 100 mA trapping and release. These two plots show the same data plotted in two useful ways. The trap-release sequence is: (1-2) Apply external current at 5 K. (2-3) Cool to 1 K. (3-4) Withdraw external current. The current is now trapped. (4-5) Begin warming. At point (5) the temperature has exceeded $T_c(I)$ and the trapped current begins to decay. (5-6) Current decays to zero. Inset shows SQUID signal change during 1-2 and 5-6 for different amounts of trapped current.

IV. Conclusions

We have demonstrated current trapping of up to 150 mA in a superconducting Nb loop using Ta/Nb persistence shunts. The required shunt and wiring dimensions can easily be accommodated within our MMC photon detector designs. Flux creep of the trapped current was unmeasurably small. The trapped current was robust against ADR regenerations at 2 K and the associated thermal, mechanical and electrical disturbances. It appears likely that this approach could also be used for standard ADRs with ~4 K regeneration temperatures, given suitable adjustments to the passive persistent shunt designs.

REFERENCES

[1] A. Fleischmann, C. Enss, and G. M. Seidel, "Metallic magnetic calorimeters," in *Cryogenic Particle Detection*, C. Enss, Ed. Berlin: Springer-Verlag, 2005, pp. 151-216.

[2] A. C. Leuthold, R. T. Wakai, G. K. G. Hohemwarter, and J. E. Nordman, "Characterization of a simple thin-film superconducting switch," *IEEE Trans. Appl. Supercond.*, vol. 4, no. 3, pp. 181-183, Sep. 1994.

[3] P .Balchandani, R. H. Torii, and R. Shile, "Thin-film persistent current switch," *IEEE Trans. Appl. Supercond.*, vol. 15, no. 3, pp. 3821-3826, Sep. 2005.

[4] V. Zakosarenko, R. Stolz, L. Fritzsch, H. G. Meyer, A. Fleischmann, and C. Enss, "SQUID gradiometer for ultra-low temperature magnetic microcalorimeter," *Supercond. Sci. Technol.*, vol. 16, pp. 1404–1407, Dec. 2003.

[5] R. Stolz, V. Zakosarenko, S. Anders, L. Fritzsch, H.-G. Meyer, A. Fleischmann, and C. Enss, "SQUID-gradiometers for arrays of integrated low temperature magnetic micro-calorimeters," *IEEE Trans. Appl. Superconductivity*, vol. 15, pp. 773–776, June 2005.

[6] R. Cantor, J. A. Hall, P. Blumenfeld, and S. T. P. Boyd, "Miniature thin-film superconducting quantum interference device susceptometer," *IEEE Trans. Appl. Supercond.*, vol. 17, no. 2, pt. 1, pp. 738–741, June 2007

[7] S. T. P. Boyd, R. Cantor, V. Kotsubo, P. Blumenfeld, and J. A. Hall, "Characterization of a miniature thin-film SQUID susceptometer for metallic magnetic microcalorimetry," *J. Low Temp. Phys.*, vol. 151, no. 1-2, pp. 369-374, Apr. 2008.

[8] S. T. P. Boyd, V. Kotsubo, R. Cantor, A. Theodorou, and J. A. Hall, "Miniature thin-film SQUID susceptometer for magnetic microcalorimetry and thermometry," *IEEE Trans. Appl. Supercond.*, vol. 19, pp. 697–701, June 2009.

[9] H. Rotzinger, J. Adams, S. R. Bandler, J. Beyer, H. Eguchi, E. Figueroa-Feliciano, W. Hsieh, G. M. Seidel, and T. Stevenson, "Performance of micro-fabricated magnetic calorimeters arrays for X-ray spectroscopy," J. Low Temp. Phys., vol. 151, no. 1/2, pp. 351–356, 2008.

[10] S. R. Kim, J. Choi, and H. S. Jo *et al*., "Development of metallic magnetic calorimeters with a critical temperature switch*," J. Low. Temp. Phys.*, vol. 184, pp. 356-362, July 2016.

[11] H. Bhang *et al*.,"AMoRE experiment: a search for neutrinoless double beta decay of ^{100}Mo isotope with $^{40}Ca^{100}MoO_4$ cryogenic scintillator detector," *J. Phys.: Conf. Ser.*, vol. 375, no. 4, Article ID 042023, 2012.

[12] http://starcryo.com

[13] D. W. Face, S. T. Ruggiero, and D. E. Prober, "Ion-beam deposition of Nb and Ta refractory superconducting films," *J. Vac. Sci. Technol. A*, vol. 1, no. 2, pp. 326-330, Apr. 1983.

[14] D. W. Face and D. E. Prober, "Nucleation of body-centered-cubic tantalum films with a thin niobium underlayer," *J. Vac. Sci. Tech. A*, vol. 5, pp. 3408–3411, Nov. 1987.

[15] D. W. Face, "Quantum limited detection and noise in superconducting tunnel junction mixers," Ph.D. dissertation, Yale Univ., New Haven, CT, 1987.

[16] M. H. Carpenter, S. Friedrich, J. A. Hall, J. Harris, and W. K. Warburton, "Development of Ta - Based Superconducting Tunnel Junction X - ray Detector Arrays," *IEEE Trans. Appl. Supercond.*, vol. 23, no. 3, p. 2400504, 2013.

[17] S. Friedrich, J. Harris, W. K. Warburton, M. H. Carpenter, J. a. A. Hall, and R. Cantor, "112-Pixel Arrays of High-Efficiency STJ X-Ray Detectors," *J. Low Temp. Phys.*, vol. 176, no. 3–4, pp. 553–559, Mar. 2014.

[18] http://starcryo.com/stj-x-ray-spectrometers/

[19] Conductus iMAG SQ1020 S/N 174, manufactured in 1995